Resonances in the Photo-ionization Continuum of Ar I (20–150 eV)*

R. P. Madden. D. L. Ederer, and K. Codling †
National Bureau of Standards, Washington, D.C.
(Received 21 June 1968)

The absorption spectrum of argon in the region 600–80 Å (20–150 eV) has been studied photographically and photoelectrically, using synchrotron light as a background source and a resolution of 0.06 Å. Many resonances have been observed in the photo-ionization continuum, which are caused by electronic excitation to auto-ionizing states of Ar I. In the region between 27 and 40 eV the observed structure is due to two types of electronic excitation: (i) the excitation of a single $3s$ electron, resulting in the configuration $3s\,3p^6\,np$ and (ii) the excitation of two of the outer $3p$ electrons simultaneously, resulting in configurations of the type $3s^2 3p^4\,nl\,n'l'$. Between 44 and 59 eV, weak structures have been observed in the absorption continuum because of the simultaneous excitation of a $3s$ and a $3p$ electron, resulting in configurations of the type $3s\,3p^5\,nl\,n'l'$. All of the observed resonances have been tabulated, and a partial classification has been given. The profiles of the resonances involving states $3s\,3p^6\,np\ {}^1P_1^\circ$, for $n=4$, 5, and 6, and the two-electron excitation states $3s^2 3p^4(^3P)4s(^2P_{3/2})4p$ and $3s^2 3p^4(^3P)3d(^2P_{3/2})4p$, have been studied quantitatively. The values of q, ρ^2, and Γ have been determined for each of these resonances, and the continuum cross section has been measured between 24 and 36 eV.

I. INTRODUCTION

The lowest ionization limits for neutral argon belong to a ^2P term of the ion. The lower level ($^2P_{3/2}$) is 15.76 eV above the ground state of Ar I, and the spin-orbit splitting is 0.18 eV. Between these two limits Beutler[1] observed, in absorption, structure due to high-series members converging onto the upper limit. These high-lying members auto-ionize owing to the interaction with the continua having an onset at the lower $^2P_{3/2}$ limit. Since Beutler's observations, several others[2–5] have examined these auto-ionizing levels by absorption techniques, or by measuring the photo-ion current directly.[6] Before 1963, these were the only known resonance structures in the photo-ionization continuum of Ar I.

Additional discrete structure in the absorption of Ar I, at higher energies, was discovered[7] in 1963, when the National Bureau of Standards' 180-MeV electron synchrotron was first utilized as a continuum background source for gas-absorption spectroscopy. At that time, a series of resonances of the reduced absorption or "window" type were reported, beginning 10.86 eV above the lowest ionization limit of argon, and converging onto the $3s\,3p^6\ {}^2S_{1/2}$ level of Ar II. These resonances were identified as being due to the single-electron excitation states $3s\,3p^6 np\ {}^1P_1^\circ$. It was indicated then that additional discrete features had been seen in the photo-ionization absorption spectrum of argon. These additional features occurred mostly at higher energies and were thought to be due to the excitation of two electrons simultaneously. Subsequently a portion of this two-electron absorption spectrum was presented with very little analysis.[8]

This paper is the final report of our observations on the resonances in argon, covering the spectral region 20 – 150 eV. As such it is the third of a series on resonances in the rare gases in this spectral region. Similar studies on helium[9] and neon[10] have been completed. We present here an analysis of the one-electron excitation structure and a partial and tentative analysis of the complex two-electron excitation resonance structure in argon.

It is important to emphasize the incomplete nature of this work. The two-electron excitation states in argon are simply not understood at present. Extensive theoretical calculations will be required to fully interpret the observed spectrum. Our tentative assignments, and the supporting arguments given below, may serve as a useful preliminary guide to those who undertake these calculations. *A priori* it might be assumed that the analysis of the two-electron spectrum in neon[10] would provide a useful guide to the similar analysis in argon. However, an outer p electron in argon can be excited to a d state without advancing in principle quantum number, and unlike the two-electron transitions in neon, those in argon readily violate L-S coupling. Thus the analysis is considerably more complicated.

We have also obtained, using a scanning photoelectric monochromator, the detailed profiles of the most prominent resonances, and have thereby determined the values of the q, Γ, and ρ^2 parameters of the Beutler-Fano[11] profiles which best describe them. As a by-product of these studies of the resonance profiles, we have determined the background photo-ionization cross section between and near the discrete structures. These results can of course be compared with numerous previous measurements,[2–4, 12–19] of which the most recent are those of Rustgi[18] and Samson.[19] Samson,[20] using a source having many closely spaced lines, has also been able to measure the cross-section at several points within the first, broad, one-electron excitation resonance ($3s\,3p^6\,4p\ {}^1P_1^\circ$). These measurements along with the spectrogram of Ref. 7 allowed a preliminary estimate of the profile parameters of this resonance.[21]

Since the first report of these resonance structures, the excitation of argon in this energy range has been studied with excitation by collision with electrons[22] and positive ions.[23] Many resonances have been observed, and a few of these have cor-

related well with the optically observed features – notably the stronger one-electron excitation features. In general, however, a close correlation between the results of the photon and particle excitation experiments does not exist. This is not surprising since in particle excitation optical selection rules need not be obeyed. Further the high resolution and photographic techniques of optical spectroscopy allow an examination of narrower and weaker structures than has been possible thus far in the particle experiments. As a result, with very few exceptions, the resonances reported here for photon excitation have not yet been identified in the particle excitation experiments.

In the presentation below, we first present the spectral positions of the resonances and the spectral analysis that has been possible. The later sections refer to the resonance profiles and the quantitative cross-section measurements.

II. EXPERIMENTAL

The most essential component of instrumentation used in these measurements was the 180-MeV electron synchrotron at the National Bureau of Standards. This source[24] provides a continuum background for absorption spectroscopy which is completely free of emission lines or any other fine structure. We have found this background source useful for absorption spectroscopy down to about 60 Å. On the long wavelength end our instruments are limited at roughly 600 Å. (The synchrotron "light" actually extends up into the visible with good strength; however, other sources of continuum are readily available above 600 Å.[25])

We have used two spectrometers in this study – both of which were specifically designed for compatibility with the synchrotron. One is a 3-m grazing-incidence spectrograph; the other a 3-m grazing-incidence scanning monochromator using photoelectric detection. Details of these instruments are discussed elsewhere.[26] In the present experiments, both were operated with a spectral slit width of approximately 0.06 Å.

The experimental techniques used to obtain the primary data are essentially identical to those used in the study of neon.[10] The gas to be studied is put directly into the spectrometers, and the absorption path is the optical path from entrance slit to exit slit or plate holder. The pressures, measured by a McLeod gauge, ranged from 5×10^{-3} to 0.3 Torr.

The spectrograph utilized Eastman SWR Schumann-type plates. Wavelength calibration was obtained by superimposing on the argon spectrum the absorption spectra of helium and neon. It has been established[26] that the wavelength positions in this instrument are reliably predicted by the grating equation. This equation has been checked against the calibration points, normalized by Minnhagen's[27] value for the limit of the $3s\,3p^6np\ {}^1P_1{}^\circ$ series, and then used to determine the wavelengths of the observed resonances.

The monochromator utilized a magnetic multiplier with a tungsten photocathode, and was operated in a counting mode. Rates were typically 500 counts/sec, and counts were stored for integration periods of the order of 2 sec. The monochromator was scanned continuously with rates on the order of 0.3 Å/min. The wavelength calibration was provided by photographic measurements on the identical spectra using the 3-m spectrograph. To reduce the effects of fluctuations in the synchrotron radiation, the ratio of the output of the ultraviolet detector to the output of a detector that monitored the synchrotron light in the visible region was recorded. The methods used to reduce the data on resonance profiles and to compare experimental and theoretical profiles are of some interest and will be published in detail elsewhere.[28] However, they will be briefly outlined in Sec. V, where the measurements on profiles are presented.

III. SPECTRA

The absorption spectrum of argon was examined photographically from 600 to 80 Å. Discrete structure was observed in the photoionization continuum between 466 Å and about 210 Å. The resonance at 466 Å is due to the lowest possible optically allowed excitation for an inner subshell electron in argon, namely $3s^2\,3p^6 \rightarrow 3s\,3p^6 4p$. The lowest-energy transition for a two-electron excitation which has been found lies at 427 Å. No resonances of any kind have been seen between 466 and 600 Å. In view of the assignments presented below it appears safe to assume that no resonance structure will exist in the optical absorption of argon at longer wavelengths until the upper level of the ionization limit ($3s^2\,3p^5\ {}^2P_{1/2}$) is reached.

Towards short wavelengths, the contrast of the structure with the continuous absorption becomes low and fades away below 210 Å. From here to the limit of our observations at 80 Å no structure has been observed. It is probable that, if detectable at all, only extremely low-contrast structure will exist from 80 Å toward shorter wavelengths, until the inner-shell $2p$ electron is excited near 51 Å.[29, 30]

The structure observed in the region 320–460 Å is shown in Fig. 1. The lowest-energy features are the prominent Rydberg series of "window" resonances to the right in Fig. 1, which are caused by the excitation of the $3s$ electron in argon. All of the remaining structure is due to the excitation of two of the outer $3p$ electrons. Window-type, absorption-type, and asymmetric resonance profiles can be seen in this complex spectrum. Below 320 Å and off Fig. 1 to the left, the structure becomes even weaker in contrast with the continuum background and fades out completely near 300 Å. Although we have not attempted to show these weak features, their positions are included in the tables. More structure appears between 276 and 210 Å, where a number of resonances exist attributed to the simultaneous excitation of $3s$ and a $3p$ electron. These absorption-type features are shown in Fig. 2.

The lowest-lying two-electron excitation states cause resonances which overlie the prominent Rydberg series of window resonances to the right

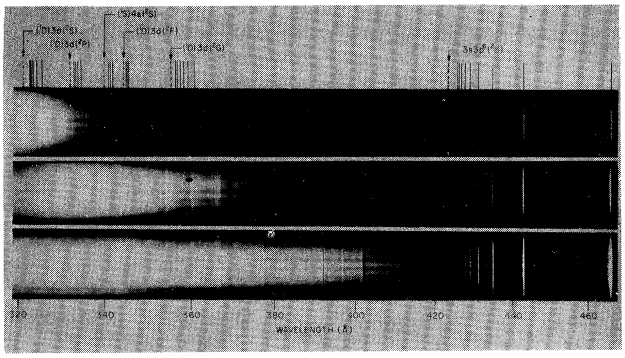

FIG. 1. Argon absorption spectrum between 320 and 470 Å taken at three different pressures to accentuate various regions of the spectrum (the background continuum cross section in this region varies by a factor of 5). This is a positive print so that black denotes absorption. The prominent series of window resonances on the right is due to the excitation of a subshell $3s$ electron to outer p orbitals. The other resonances are due to the simultaneous excitation of two $3p$ electrons. A few of the levels of Ar II to which Rydberg series of resonances have been seen are indicated on the figure at the upper left.

in Fig. 1. These weaker features can best be seen in Fig. 3, which is a densitometer trace of the high members of the series. Here a weak satellite can be distinguished on the long-wavelength side of the intensity-perturbed $n = 10$ member of the $3s\ 3p^6 np\ {}^1P_1{}^\circ$ series. Also note that at shorter wavelengths, where the main series becomes unresolved, there is a significant decrease in absorption owing to a second overlapping two-electron excitation resonance.

Figure 4 is a densitometer trace of a broader spectral region, showing the more prominent two-electron excitation resonances. Note the sharpness of these features and the variety of profiles which exist.

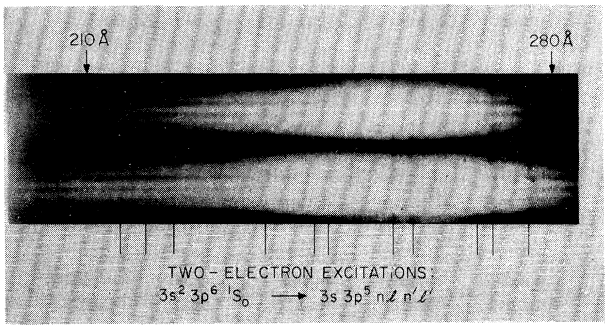

FIG. 2. Argon absorption spectrum between 200 and 280 Å showing two-electron excitations to states of the configurations $3s\ 3p^5\ nl\ n'l'$, which appear as weak absorption-type resonances. The vertical lines indicate the positions of some of the stronger features.

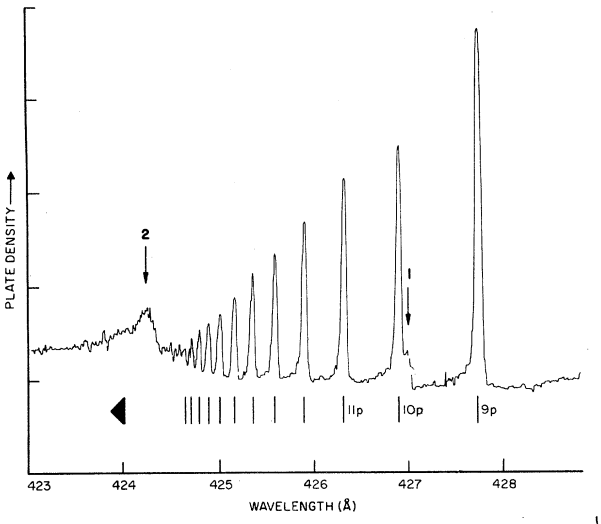

FIG. 3. A densitometer trace of the higher members of the $3s\ 3p^6\ np\ {}^1P_1{}^\circ$ series of window-type resonances. The intensity perturbation of the $n = 10$ series member by the $({}^3P)4s({}^2P_{3/2})4p$ resonance (1) can be clearly seen. Resonance (2), classified as $({}^3P)4s({}^2P_{1/2})4p$ is superimposed on the unresolved higher members of the $3s\ 3p^6\ np\ {}^1P_1{}^\circ$ series.

IV. CLASSIFICATION OF SPECTRA

A. One-electron Excitation

The prominent Rydberg series of window-type resonances to the right in Fig. 1 converge onto the known $3s\ 3p^6\ {}^2S_{1/2}$ level of Ar II, and can be associated with the transitions, $3s^2\ 3p^6\ {}^1S_0 \rightarrow 3s\ 3p^6 np\ {}^1P_1{}^\circ$.

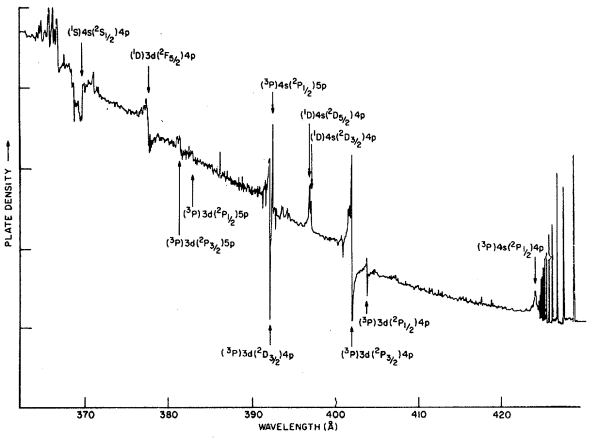

FIG. 4. A densitometer trace of a portion of the spectrum shown in Fig. 1, showing the more prominent two-electron excitation resonances. Asymmetric-, window-, and absorption-type profiles can be seen. The classification of a number of these resonances is indicated.

It is well known that transitions in Ar I involving excitation of a $3p$ electron do not obey L-S coupling rules. (Note that the $3p$ splitting of the lowest-ionization limit is over 1400 cm^{-1}.) However, in the case encountered here, a subshell $3s$ electron is being excited. While two $J=1$ levels of the excited configuration are available, an intermediate coupling calculation indicates that each level can be described either as almost pure $^1P_1$ or $^3P_1$ with only an 8% admixture of the other. It is, therefore, a good approximation to label the single observed series converging to the $3s\,3p^6\ ^2S_{1/2}$ level in Ar II as $^1P_1$. If a second weak series exists the spin-orbit splitting would be of the order of the resonance width, and hence the weak series would be physically merged with the main series.

The observed resonances which are members of this series are listed in Table I. The observed wavelength is given along with the wave number and effective quantum number. The quantum defect for this series is about double that found for the similar series in Ne I.[10]

A calculation[31] of the energy of the $3s\,3p^6\,4p\ ^1P_1^\circ$ level from first principles has been made by A. Weiss, using Hartree-Fock wave functions. The calculation predicts the resonance at 465.6 Å in good agreement with the experimental value 465.84 ± 0.03 Å.

B. Two-electron Excitation, $3p^6 \rightarrow 3p^4 nln'l'$

It can be concluded that the remainder of the spectra seen in Figs. 1–4 are due to two-electron excitation transitions from the following argument. There are no single-electron-excitation possibilities in this energy region other than those considered in Sec. IV A above. (The next-highest-energy one-electron excitation is that of a $2p$ electron,[29,30] which occurs at a photon energy of 250 eV.) Thus the remaining structures observed in this investigation are due to the simultaneous excitation of more than one electron. Three-electron excitations are ruled out because the energy available is not sufficient to allow such an explanation except for the highest-energy resonances observed. Furthermore none were found in neon, and if present in argon, they would be expected to be weaker than the two-electron transitions by one or two orders of magnitude.

Let us first consider wavelengths longer than 286 Å (or an energy of 43.4 eV – the lowest threshold for producing Ar^{++}). In this region the two-electron states may involve excitation of two of the outer p electrons in the following way: $3s^2\,3p^6\ ^1S_0 \rightarrow 3s^2\,3p^4 nl\,n'l'$.

From a consideration of two-electron excitation selection rules,[32] the following transitions are most probable:

$$3s^2\,3p^6 \rightarrow 3s^2\,3p^4\,3d\,np$$
$$3d\,nf$$
$$4snp$$
$$4snf$$
$$4pns$$
$$4pnd$$
$$4fns$$
$$4fnd.$$

Of these possibilities, only those involving an f electron require that both electrons change angular momentum. While such transitions might be expected to be weaker than the others, we have experimental evidence of resonances due to excitation of such configurations.

All of the above configurations have a common "grandparent" configuration. The four equivalent p electrons yield terms of the type $3s^2\,3p^4$ ($^3P, ^1D, ^1S$). The final-term possibilities are then determined by adding on the two remaining electrons. Considering only the first four electron configurations listed above, we arrive at the results shown in the Term Arrays in Table II.

In these arrays, the parent terms are formed from the grandparent terms on the same horizontal line by the addition of the indicated electron. The addition of the second electron yields the arrays at the right which have the following interpretation. These final-state arrays have the same number of elements on each line as the parent arrays. The numerical value of each element represents the number of $J=1$ levels which can be formed from the corresponding parent term by the addition of the indicated electron. The asterisk on some of the elements means that one of that number of final $J=1$ levels would be a $^1P_1$ level if L-S coupling prevailed. The parenthetical number for each element represents the number of $J=1$ levels for which we feel there is experimental evidence. The discussion below will consider these parenthetical numbers in greater detail.

Similar term arrays can easily be constructed for the remaining configurations listed above, namely, $4pns$, $4pnd$, $4fns$, and $4fnd$. However, experimental evidence on these configurations is

TABLE I. Principal quantum number n, wavelength λ, wave number ν, and effective principal quantum number n^*, for members of the $3s^2\,3p^6\ ^1S_0 \rightarrow 3s\,3p^6 np\ ^1P_1^\circ$ series in Ar I. The wavelengths were determined at the point of maximum transmission. The error quoted represents the estimated probable error.

n	λ(Å)	ν (cm^{-1})	n^*
4	465.83 ± 0.03	214 672	2.277
5	442.83 ± 0.01	225 818	3.310
6	434.87 ± 0.01	229 955	4.321
7	431.10 ± 0.01	231 964	5.327
8	429.01 ± 0.01	233 094	6.33
9	427.73 ± 0.01	233 790	7.33
10	426.89 ± 0.01	234 252	8.34
11	426.31 ± 0.01	234 572	9.33
12	425.89 ± 0.01	234 804	10.33
13	425.57 ± 0.01	234 977	11.33
14	425.33 ± 0.01	235 110	12.34
15	425.14 ± 0.01	235 215	13.34
16	424.99 ± 0.01	235 298	14.34
17	424.87 ± 0.01	235 366	15.35
18	424.77 ± 0.01	235 421	16.35
19	424.69 ± 0.01	235 466	17.32
20	424.62 ± 0.01	235 504	18.31

TABLE II. Term Arrays: formed by adding a $3d$ or $4s$ electron and then a p or f electron onto the $3p^4$ (^3P, ^1D, ^1S) terms of the grandparent. Elements of final arrays show the number of $J=1$ levels available (the number for which there is experimental evidence is in parentheses) – an asterisk indicates that a $^1P_1$ level is present in L–S coupling.

$3p^4$	^3P, ^1D, ^1S	$3d$	^2P, ^2D, ^2F, ^4P, ^4D, ^4F ^2S, ^2P, ^2D, ^2F, ^2G ^2D	np	4*(4), 3*(3), 1(1), 5(2), 5(0), 3(0) 2*(1), 4*(1), 3*(1), 1(1), 0 3*(2)
$3p^4$	^3P, ^1D, ^1S	$3d$	^2P, ^2D, ^2F, ^4P, ^4D, ^4F ^2S, ^2P, ^2D, ^2F, ^2G ^2D	nf	1(0), 3*(1), 4*(1), 3(0), 5(0), 6(0) 0, 1(0), 3*(0), 4*(1), 3*(1) 3*(0)
$3p^4$	^3P, ^1D, ^1S	$4s$	^2P, ^4P ^2D ^2S	np	4*(4), 5(0) 3*(2) 2*(1)
$3p^4$	^3P, ^1D, ^1S	$4s$	^2P, ^4P ^2D ^2S	nf	1(0), 3(1) 3*(1) 0

rather meager. Hence the corresponding term arrays are rather academic and will not be given, although the experimental data which may be attributed to these configurations will be indicated below.

In analyzing the two-electron excitation spectrum of Ne I, it was found[10] that L-S coupling held quite well, while the ordinary Ne I energy-level structure shows jl coupling. The two-electron excitation spectrum of Ar I is too rich in structure to be explained on a basis of L-S coupling. On the other hand not all of the $J=1$ levels indicated in the Term Arrays of Table II have given rise to observable structure. Thus our approach has been to look for a strong $J=1$ level in the asterisked elements, and to expect other $J=1$ levels as well. Assuredly the final levels to which transitions can be observed must contain some $^1P_1$ character, since the initial (ground) level for all observed transitions is pure $^1S_0$.

Crude estimates of the expected positions of the resonances can be obtained from the known levels of the ion and typical quantum defects for s, p, d, and f electrons. However, with such a rich spectrum and because of the screening and configuration-interaction effects, such estimates are not sufficiently accurate to establish definite assignments. Good theoretical calculations are made difficult by the breakdown in L-S coupling. Hence the assignments which have been made are on the basis of resonance shape, width and intensity, the consistency of the quantum defects for a series, the ion level to which a series converges (if the convergence limit can be established), and the anticipated more probable configurations.

For some series, only high-lying members have been found – for others only low-lying members. Intensity-sharing interactions of the various two-electron configurations appear to be primarily responsible for such effects. Also high-lying members may be too weak, or low-lying members too broad, to be distinguished. Sometimes these effects result in a series having intermediate members missing, a phenomenon previously observed in neon[10] and in barium.[33]

These many difficulties have made a highly reliable classification of the two-electron spectrum of Ar I impossible at this time. A significant portion of the classification suggested below may require future revision, which can be done as reliable theoretical calculations of the energies of the two-electron excitation states become available.

From the above term analysis, we see that the configuration $3s^2 3p^4\, 3dnp$ has a total of thirty-four $J=1$ levels and thus 34 possible Rydberg series. Similarly the configuration $3s^2\, 3p^4\, 4pnd$ would have thirty four $J=1$ levels, and the Rydberg series for these two configurations would have first members in common, corresponding to the levels of $3d\,4p$. In the same manner, the terms of $4snp$ have a total of fourteen $J=1$ levels, thus 14 possible Rydberg series with first members common to to those of $4pns$; and so on, for the remaining configurations. The experimental fact is, however, that such a rich spectrum does *not* develop, and *excited configurations of the type* $3p^4\,3dnl$ and $3p^4\,4snl$ *dominate the spectrum.*

Table III is a list of all the observed two-electron excitation resonances in order of their appearance in the spectrum. The wavelengths and profile types are indicated along with the suggested classification when possible. Let us now consider the experimental evidence and classification in greater detail.

1) $3s^2\,3p^4\,3dnp$; $3s^2\,3p^4\,3dnf$

These configurations, having the same parent term systems, will be treated together. Of the two, the $3dnp$ configuration would be expected to be the more prominent in the spectrum, since only one electron is required to change angular momentum. The resonances which have been classified as belonging to these configurations are listed in Table IV(a). In this table, the configurations and parent terms are listed in the order of their occurrence in the above Term Arrays (Table II). The principle quantum number n and the effective

TABLE III. Code number, wavelength λ, and profile type for all the observed resonances which are due to electron transitions of the type $3s^2\,3p^6 \rightarrow 3s^2\,3p^4\,nl\,n'l'$, listed in order of their occurrence in the spectrum. The resonances are typed as follows: As, asymmetric type – a minus sign indicates the resonance has a negative q; W, window type; A, absorption type. This evaluation is qualitative and performed by visual inspection of the spectra. In fact, all resonances are probably asymmetric to some extent. The error limit represents the estimated probable error. All asymmetric resonances were measured at the point where the rate of change in the plate density was greatest, unless otherwise stated. Classifications which are very tentative are followed by a question mark.

Code	λ(Å)	Type	Identification
1	426.99 ± 0.02	As(–)	$(^3P)4s(^2P_{3/2})4p$
2	424.23 ± 0.02	As(–)	$(^3P)4s(^2P_{1/2})4p$
3	403.90 ± 0.02	As(–)	$(^3P)3d(^2P_{1/2})4p$
4	403.69 ± 0.02	As(–)	$(^3P)3d(^2P_{1/2})4p$
5	401.92 ± 0.02[a]	As(–)	$(^3P)3d(^2P_{3/2})4p$
6	401.59 ± 0.02	W	$(^3P)3d(^4P_{1/2})4p$
7	401.45 ± 0.02	W	$(^3P)3d(^4P_{3/2})4p$
8	400.77 ± 0.02	As(–)	$(^3P)3d(^2P_{3/2})4p$
9	396.99 ± 0.02	W	$(^1D)4s(^2D_{3/2})4p$
10	396.76 ± 0.02	W	$(^1D)4s(^2D_{5/2})4p$
11	394.35 ± 0.03	W	$(^3P)4s(^2P_{3/2})5p$
12	394.16 ± 0.02	W	$(^3P)4s(^2P_{3/2})5p$
13	393.51 ± 0.03	W	$(^3P)4s(^4P_{5/2})4f$
14	392.73 ± 0.03	A	$(^3P)3d(^2F_{5/2})4p$
15	392.33 ± 0.03	W	$(^3P)4s(^2P_{1/2})5p$
16	392.17 ± 0.02	As(–)	$(^3P)4s(^2P_{1/2})5p$
17	392.06 ± 0.03[a]	As(–)	$(^3P)3d(^2D_{3/2})4p$
18	391.52 ± 0.02	A	$(^3P)3d(^2D_{3/2})4p$
19	391.17 ± 0.02	A	$(^3P)3d(^2D_{5/2})4p$
20	386.34 ± 0.03	W	$(^3P)4s(^2P_{3/2})6p$
21	386.08 ± 0.03	W	$(^3P)4s(^2P_{3/2})6p$
22	382.82 ± 0.03	As(–)	$(^3P)3d(^2P_{1/2})5p$
23	381.29 ± 0.03	As(–)	$(^3P)3d(^2P_{3/2})5p$
24	381.07 ± 0.03	W	$(^3P)3d(^2P_{3/2})5p$
25	377.76 ± 0.02	W	• • •
26	377.63 ± 0.03	W	• • •
27	377.54 ± 0.03	W	$(^1D)4s(^2D_{3/2})5p$
28	377.40 ± 0.02	As(–)	$(^1D)3d(^2F_{5/2})4p$
29	377.24 ± 0.04	As(–)	$(^1D)4s(^2D_{5/2})5p$
30	371.89 ± 0.04	As(–)	$(^1D)4s(^2D_{5/2})4f$
31	371.31 ± 0.02	As(–)	$(^3P)3d(^2F_{7/2})4f$
32	370.57 ± 0.05	A	$(^3P)4p(^4D_{3/2})5s$?
33	370.31 ± 0.02	A	$(^3P)4p(^4D_{1/2})5s$?
34	369.93 ± 0.02	As(+)	$(^1S)4s(^2S_{1/2})4p$
35	369.20 ± 0.04	A	$(^3P)4p(^2D_{3/2})5s$
36	369.00 ± 0.02	A	$(^3P)4p(^2P_{1/2})5s$
37	368.78 ± 0.04	As(–)	$(^3P)4p(^2P_{3/2})5s$
38	367.83 ± 0.02	As(–)	$(^3P)3d(^2F_{7/2})5f$
39	366.99 ± 0.02	As(–)	• • •
40	366.73 ± 0.02	W	$(^3P)4p(^2S_{1/2})5s$?
41	366.51 ± 0.02	As(–)	• • •
42	366.05 ± 0.02	As(–)	$(^1D)4s(^2D_{5/2})8p$
43	365.65 ± 0.02	W	• • •
44	365.17 ± 0.02	As(–)	$(^1D)4s(^2D_{5/2})9p$
45	364.95 ± 0.02	W	• • •
46	364.70 ± 0.02	W	• • •
47	364.47 ± 0.02	W	$(^1D)4s(^2D_{5/2})10p$
48	363.42 ± 0.04	As(–)	$(^3P)3d(^2D_{5/2})6f$
49	363.36 ± 0.04	As(–)	$(^3P)3d(^2D_{5/2})7f$

TABLE III (*continued*)

Code	λ(Å)	Type	Identification
50	361.28 ± 0.02	As(+)	$(^1D)3d(^2G_{7/2})5f$
51	360.30 ± 0.04	W	$(^1D)3d(^2P_{3/2})4p$
52	359.44 ± 0.02	As(–)	$(^1D)3d(^2G_{7/2})6f$
53	358.38 ± 0.02	As(–)	$(^1D)3d(^2G_{7/2})7f$
54	357.68 ± 0.02	As(–)	$(^1D)3d(^2G_{7/2})8f$
55	357.22 ± 0.02	As(–)	$(^1D)3d(^2G_{7/2})9f$
56	356.88 ± 0.02	As(–)	$(^1D)3d(^2G_{7/2})10f$
57	356.65 ± 0.02	As(–)	$(^1D)3d(^2G_{7/2})11f$
58	356.0 ± 0.10	W	• • •
59	354.30 ± 0.02	W	$(^1S)3d(^2D_{5/2})4p$
60	352.97 ± 0.02	W	$(^1S)3d(^2D_{3/2})4p$
61	352.63 ± 0.04	W	$(^1D)4p(^2P_{3/2})5s$?
62	352.08 ± 0.02	W	$(^3P)4p(^2D_{3/2})9s$
63	351.58 ± 0.02	W	$(^1D)4p(^2P_{1/2})5s$?
64	351.27 ± 0.02	W	$(^3P)4p(^2D_{3/2})10s$
65	350.97 ± 0.02	W	$(^1D)4p(^2D_{3/2})5s$?
66	350.83 ± 0.02	W	$(^3P)4p(^2D_{3/2})11s$
67	349.68 ± 0.05	W	• • •
68	349.34 ± 0.03	As(–)	• • •
69	348.15 ± 0.05	As(–)	• • •
70	346.75 ± 0.03	As(+)	$(^1S)4s(^2S_{1/2})6p$
71	345.72 ± 0.03	A	$(^1D)3d(^2F_{7/2})9f$
72	345.42 ± 0.05	A	$(^1D)3d(^2F_{7/2})10f$
73	345.21 ± 0.05	A	$(^1D)3d(^2F_{7/2})11f$
74	344.21 ± 0.02	A	$(^1S)4s(^2S_{1/2})7p$
75	343.5 ± 0.10	A	• • •
76	342.83 ± 0.03	As(–)	$(^1S)4s(^2S_{1/2})8p$
77	342.05 ± 0.03	A	$(^1S)4s(^2S_{1/2})9p$
78	341.50 ± 0.03	A	$(^1S)4s(^2S_{1/2})10p$
79	341.14 ± 0.05	A	$(^1S)4s(^2S_{1/2})11p$
80	340.85 ± 0.05	A	$(^1S)4s(^2S_{1/2})12p$
81	340.50 ± 0.03	W	• • •
82	340.1 ± 0.10	A	• • •
83	338.93 ± 0.03	A	• • •
84	338.1 ± 0.10	W	$(^1S)3d(^2D_{5/2})5p$
85	337.08 ± 0.03	W	$(^1D)3d(^2D_{5/2})8p$
86	336.30 ± 0.05	W	$(^1D)3d(^2D_{5/2})9p$
87	335.68 ± 0.03	W	• • •
88	335.27 ± 0.03	A	• • •
89	334.77 ± 0.03	W	$(^1D)3d(^2P_{3/2})8p$
90	333.95 ± 0.02	W	$(^1D)3d(^2P_{3/2})9p$
91	333.42 ± 0.02	W	$(^1D)3d(^2P_{3/2})10p$
92	333.07 ± 0.04	W	$(^1D)3d(^2P_{3/2})11p$
93	332.50 ± 0.02	As(–)	$(^1S)3d(^2D_{5/2})6p$
94	330.45 ± 0.04	W	$(^1S)3d(^2D_{5/2})7p$
95	329.45 ± 0.05	W	• • •
96	329.02 ± 0.05	W	• • •
97	327.65 ± 0.04	As(–)	• • •
98	327.30 ± 0.04	As(–)	• • •
99	325.63 ± 0.04	A	$(^1D)3d(^2S_{1/2})7p$
100	324.37 ± 0.04	A	$(^1D)3d(^2S_{1/2})8p$
101	323.52 ± 0.04	A	$(^1D)3d(^2S_{1/2})9p$
102	323.00 ± 0.04	A	$(^1D)3d(^2S_{1/2})10p$
103	322.68 ± 0.04	A	$(^1D)3d(^2S_{1/2})11p$
104	319.68 ± 0.04	A	• • •
105	319.03 ± 0.04	A	$(^3P)4d(^2P_{1/2})7p$?
106	317.98 ± 0.04	A	$(^3P)4d(^2P_{1/2})8p$?
107	317.34 ± 0.04	A	$(^3P)4d(^2P_{1/2})9p$?
108	316.45 ± 0.03	A	• • •
109	316.10 ± 0.04	A	• • •
110	315.54 ± 0.05	A	• • •
111	314.77 ± 0.05	A	$(^3P)4d(^2D_{5/2})9p$?
112	314.35 ± 0.05	A	$(^3P)4d(^2D_{5/2})10p$?
113	313.26 ± 0.03	A	• • •
114	311.46 ± 0.05	A	$(^1D)5s(^2D_{3/2})9p$?

TABLE III (*continued*)

Code	λ(Å)	Type	Identification
115	311.07 ± 0.05	A	$(^1D)5s(^2D_{3/2})10p$?
116	310.7 ± 0.10	A	• • •
117	308.99 ± 0.05	A	$(^1D)4d(^2D_{3/2})7p$?
118	308.1 ± 0.10	A	$(^1D)4d(^2D_{3/2})8p$?
119	307.6 ± 0.10	A	• • •
120	305.6 ± 0.10	W	• • •
121	304.2 ± 0.10	W	• • •
122	303.25 ± 0.05	A	• • •
123	302.4 ± 0.10	A	• • •
124	301.1 ± 0.10	A	• • •
125	300.7 ± 0.10	A	• • •
126	300.3 ± 0.10	A	• • •
127	298.2 ± 0.10	A	• • •
128	297.5 ± 0.10	A	• • •
129	296.7 ± 0.10	A	• • •
130	295.5 ± 0.10	A	• • •
131	295.2 ± 0.10	A	• • •
132	291.8 ± 0.10	A	• • •
133	291.1 ± 0.10	A	• • •

[a]Measured at peak absorption point.

quantum number n^* consistent with the suggested classification are also given. The numbers listed in the third column correspond to the resonance code number in Table III. Table III can, therefore, be consulted to obtain information on the type and wavelength of the resonances.

From Table IV(a), it can be seen that few Rydberg series are well developed. In the case of the $3dnp$ series associated with the (^3P) grandparent, no series members with $n > 5$ have been located. This is true even for the $(^3P)3d(^2P_{3/2})np$ series, to which has been assigned the strongest feature of the two-electron excitation spectrum of argon.

Note that almost all of the assignments of final states which have been possible involve the parent terms which can form $^1P_1$ levels with an added p or f electron. In other words, there may be more than one $J = 1$ level, but the preferred final states are those which are most closely associated with the $^1P_1$ levels which would be formed in L-S coupling. This rule holds quite well for the doublet terms of the parent, where the only exceptions are the assignments $(^3P)3d(^2F)4p$ and $(^1D)3d(^2F)4p$. These states do not form $^1P_1$ levels, but apparently enter into interactions which allow them to borrow some $^1P_1$ character.

Note also that transitions to configurations containing a p or f electron added onto the quartet terms of the ion are rarely observed, probably owing to the fact that one cannot form a singlet by adding one electron to a quartet term. Exceptions to this are the two $(^3P)3d(^4P)4p$ assignments. If correct, these resonances may only be visible because of an interaction with the close by and strong $(^3P)3d(^2P_{1/2})4p$ resonance (5).

In the case of the ^1D grandparent we see two well-developed Rydberg series, namely, $(^1D)3d(^2S_{1/2})np$ and $(^1D)3d(^2P_{3/2})np$. In the former, the lower-lying members could not be assigned – the problem being that this configuration, judged by the width of the resonance, is characterized by a short lifetime and the lower Rydberg series mem-

TABLE IV. Resonances grouped according to classification, following the ordering in the Term Arrays for transitions of the type $3s^2\,3p^6 \rightarrow 3s^2\,3p^4\,nl\,n'l'$. The effective quantum number given is that appropriate to the suggested assignment, and the code number allows cross referencing to Table III. A "No" occurring in the n^* column means that we have not seen any resonance in the vicinity of the expected position for this classification. A question mark occurring in the n^* column means that no resonance could be found for this classification, in spite of the fact that it would seem reasonable for it to occur.

Classification	n^*	Code
(a) Resonances due to transitions of the type $3s^2\,3p^6 \rightarrow 3s^2\,3p^4\,3d\,nl$		
$3p^4(^3P)3d(^2P_{1/2})4p$	2.129	3
$4p$	2.134	4
$5p$	3.217	22
$(^2P_{3/2})4p$	2.139	5
$4p$	2.172	8
$5p$	3.231	23
$5p$	3.255	24
$4f$	No	
$(^2D_{3/2})4p$	2.207	17
$4p$	2.225	18
$5p$	?	
$4f$	No	
$(^2D_{5/2})4p$	2.206	19
$5p$	?	
$4f$	No	
$6f$	6.01	48
$7f$	7.02	49
$(^2F_{7/2})4f$	3.967	31
$5f$	4.98	38
$(^2F_{5/2})4p$	2.202	14
$5p$	?	
$4f$	?	
$(^4P_{1/2})4p$	2.081	6
$(^4P_{3/2})4p$	2.074	7
$4f$	No	
$(^4P_{5/2})4p$	?	
$4f$	No	
$(^4D)\,4p$, or $4f$	No	
$(^4D)\,4p$, or $4f$	No	
$3p^4(^1D)3d(^2S_{1/2})4p$	Too Broad[a]	
$7p$	5.17	99
$8p$	6.14	100
$9p$	7.22	101
$10p$	8.27	102
$11p$	9.25	103
$(^2P_{3/2})4p$	2.139	51
$5p$	?	
$8p$	6.25	89
$9p$	7.27	90
$10p$	8.29	91
$11p$	9.26	92
$4f$	No	
$(^2P_{1/2})4p$	?	
$(^2D_{5/2})4p$	Available[b]	
$8p$	6.28	85
$9p$	7.24	86
$4f$	No	
$(^2D_{3/2})4p$	Available	
$4f$	No	

TABLE IV (*continued*)

Classification	n^*	Code
$(^2F_{5/2})4p$	2.077	28
$4f$	No	
$(^2F_{7/2})4f$	No	
$9f$	8.97	71
$10f$	9.92	72
$11f$	10.83	73
$(^2G_{9/2})4f$	No	
$(^2G_{7/2})4f$	?	
$5f$	4.93	50
$6f$	5.95	52
$7f$	6.94	53
$8f$	7.96	54
$9f$	8.94	55
$10f$	9.95	56
$11f$	10.88	57
$3p^4(^1S)3d(^2D_{5/2})4p$	2.118	59
$5p$	3.168	84
$6p$	4.29	93
$7p$	5.18	94
$4f$	No	
$(^2D_{3/2})4p$	2.150	60
$4f$	No	
(b) Resonances due to transitions of the type $3s^2\ 3p^6 \rightarrow 3s^2\ 3p^4\ 4s\ nl$		
$3p^4(^3P)4s(^2P_{3/2})4p$	1.877	1
$5p$	3.060	11
$5p$	3.069	12
$6p$	4.10	20
$6p$	4.16	21
$4f$	No	
$(^2P_{1/2})4p$	1.892	2
$5p$	3.092	15
$5p$	3.106	16
$(^4P_{5/2})4p$	No	
$4f$	3.896	13
$(^4P_{3/2})4p$	No	
$4f$	No	
$(^4P_{1/2})4p$	No	
$3p^4(^1D)4s(^2D_{3/2})4p$	2.146	9
$5p$	3.179	27
$4f$	No	
$(^2D_{5/2})4p$	2.142	10
$5p$	3.178	29
$8p$	6.30	42
$9p$	7.22	44
$10p$	8.33	47
$4f$	3.944	30
$3p^4(^1S)4s(^2S_{1/2})4p$	2.135	34
$5p$	?	
$6p$	4.27	70
$7p$	5.31	74
$8p$	6.34	76
$9p$	7.29	77
$10p$	8.30	78
$11p$	9.25	79
$12p$	10.30	80
(c) Resonances due to transitions of the type $3s^2\ 3p^6 \rightarrow 3s^2\ 3p^4\ 4d\ nl$; $3s^2\ 3p^6 \rightarrow 3s^2\ 3p^4\ 5s\ nl$		
$3p^4(^3P)4d(^2P_{1/2})7p$	5.52	105
$8p$	6.55	106
$9p$	7.55	107
$(^2D_{5/2})9p$	7.45	111
$10p$	8.41	112

TABLE IV (*continued*)

Classification	n^*	Code
$(^1D)4d(^2D_{3/2})7p$	5.63	117
$8p$	6.60	118
$(^1D)5s(^2D_{3/2})9p$	7.59	114
$10p$	8.54	115
(d) Resonances due to transitions of the type $3s^2\ 3p^6 \rightarrow 3s^2\ 3p^4\ 4p\ ns$		
$3p^4(^3P)4p(^2S_{1/2})5s$	2.659	40
$(^2P_{1/2})5s$	2.634	36
$(^2P_{3/2})5s$	2.604	37
$(^2D_{3/2})5s$	2.649	35
$9s$	6.66	62
$10s$	7.76	64
$11s$	8.65	66
$(^4D_{3/2})5s$	2.667	32
$(^4D_{1/2})5s$	2.661	33
$3p^4(^1D)4p(^2P_{3/2})5s$	2.640	61
$(^2P_{1/2})5s$	2.661	63
$(^2D_{3/2})5s$	2.658	65

[a]This resonance could not be specifically placed. However, a consideration of the breadths of the higher series members tells us that this resonance would be too broad to be easily visible.

[b]The word "Available" in the n^* column means that there are many resonances, otherwise unclassified, which exist in the near vicinity of the expectation value for this classification. No particular selection has been made.

bers are too broad to be located. This same explanation may be applicable to the latter configuration, where members below $n = 8$ are missing with the exception of $n = 4$. In this interpretation, the $n = 4$ member might be thought of as belonging to a second $J = 1$ series, weaker and of longer lifetime.

Focusing attention on the $3d\,nf$ assignments for a moment, we see that in general these resonances are not as prominent as those for the $3d\,np$ configurations. This is expected owing to the extra angular-momentum change required, and one tends to question any such assignments. We can properly be skeptical of the fragmentary series assignments $(^3P)3d(^2D)nf$, $(^3P)3d(^2F)nf$, and $(^1D)3d(^2F)nf$; however, there can be no question of the assignment for the well-developed series $(^1D)3d(^2G_{7/2})nf$.

2) $3s^2\ 3p^4\ 4s\,np$; $3s^2\ 3p^4 4s\,nf$

These two configurations also share the same parent terms in the Term Arrays of Table II. The assignments which have been made to these configurations, along with the principle quantum number and effective quantum number consistant with the assignment are included in Table IV(b).

The configuration which can be formed from the ground state by one electron changing angular momentum ($4s\,np$) is favored over that which requires both electrons to change angular momentum. In fact the $4s\,nf$ configuration is suggested for only two of the observed resonances. One of these, $(^1D)4s(^2D_{5/2})4f$, would have a $^1P_1$ level in L-S coupling, yet the resonance is very weak.

The other assignment is $(^3P)4s(^4P_{5/2})4f$. This configuration would have no $^1P_1$ level in L-S coupling, hence the assignment appears more questionable.[34] However, the parent configuration $(3p^4ns)$ has been shown by Minnhagen[27] to exhibit, in general, strong pair coupling; and some departure from L-S coupling in the $J=\frac{5}{2}$ level of the $(^3P)4s$ configuration is to be expected. Hence there may be a significant amount of $^1P_1$ character mixed into the levels of the configuration $(^3P)4s(^4P_{5/2})4f$.

Considering the series $(^3P)4s(^2P_{3/2})np$ and $(^3P)4s(^2P_{1/2})np$ in greater detail, we note the following. The first members of these two series are the lowest-lying two-electron excitation resonances in argon. They show the usual depression in effective quantum number seen previously in neon[10] for two-electron excitation transitions. Resonance (1) causes an intensity perturbation (see Fig. 3) in the $3s\,3p^6\,10p\ ^1P_1^\circ$ resonance, without a noticeable displacement of that resonance, as shown by the consistent effective quantum number sequence in Table I. Resonance (2), the first member of the $(^3P)4s(^2P_{1/2})np$ series, appears considerably broader. This resonance is superimposed on the high members of the $3s\,3p^6np\ ^1P_1^\circ$ series which are unresolved in Fig. 3 [the point of maximum transmission of resonance (2) is at 424.23 Å while the $3s\,3p^6np\ ^1P_1^\circ$ series limit is at 424.03 Å]. A discussion of the profile of resonance (2) is given in Sec. V. B. (2).

The $n=5$ members of the $(^3P)4s(^2P_{3/2})np$ and $(^3P)4s(^2P_{1/2})np$ series each show two members; this is appropriate as there are four $J=1$ levels available. The $(^2P_{3/2})np$ series has been assigned two $6p$ members as well. Transitions to second $J=1$ levels for the $n=4$ members of these series may not have been observed owing to stronger L-S coupling for the low-series members.

A puzzling characteristic of these two series of resonances is their weakness. These transitions are to the lowest-lying two-electron excitation states in argon. By comparison, the low-lying $2s^22p^4(^3P)3s(^2P)3p\ ^1P_1^\circ$ level of neon results in the most prominent resonance in the two-electron excitation spectrum.[10]

Of the other $4snp$ series assignments in argon, the series $(^1S)4s(^2S_{1/2})np$ is the best developed, $n=4$ through $n=12$ having been assigned, although $n=5$ is missing. The series $(^1D)4s(^2D_{5/2})np$ has 5 members assigned, but also has intermediate members missing [see Table IV(b)].

Further justification for the assignment of the $n=4$ members of the $3s^2\,3p^4\,4snp$ series is provided by the theoretical calculations of A. Weiss.[31] Using Hartree-Fock wave functions and including configuration mixing, he has calculated the energies of the levels $(^3P)4s(^2P)4p\ ^1P_1^\circ$, $(^1D)4s(^2S)4p\ ^1P_1^\circ$, and $(^1S)4s(^2D)4p\ ^1P_1^\circ$ assuming L-S coupling. The predicted wavelengths of the associated resonances are 425.3, 395.2, and 369.0 Å. These compare favorably with the experimental values 424.2 and 427.0 Å for the two assigned $J=1$ levels of $(^3P)4s(^2P)4p$, with the values 396.8 and 397.0 Å for the two assigned $J=1$ levels of $(^1D)4s(^2D)4p$, and with 369.9 Å for the single observed resonance assigned to $(^1S)4s(^2S)4p$. The differences between the observed and calculated values is within the probable error of the calculations.

There are several ways to explain the observation of series which have intermediate members missing, as in the series $(^1S)4s(^2S)np$ and $(^1D)4s(^2D)np$ above. Owing to the strong mutual screening of two excited electrons in low orbits, the first-few series members have different quantum defects than the high-series members. The amount of this depression of low-series members varies with the parent and grandparent terms involved. Thus, with the second and/or third member missing, one is not able to securely tie the two ends of the series together. As mentioned earlier, it might happen that two $J=1$ series are to be associated with the same limit. If one series consisted of sufficiently broad resonances, the low members would be difficult or impossible to locate, and if the other series consisted of sharp, but much weaker resonances, then its series might experimentally disappear after one or two members. Combining these two series would give the impression of a single series with missing members.

A second possibility for the appearance of a series with members missing in the middle is that the series is in fact weak so that it disappears after one or two members. The reappearance of the series in high members might come about through an intensity sharing interaction with another overlapping configuration, as appears to be the case in neon in the $2s^22p^4(^3P)3s(^2P)np$ series.[10] Interactions of this type can be expected to be quite prevalent in auto-ionization spectra, owing to the broadness of the resonances and the many overlapping configurations.

3) *Possible series* $3s^2\,3p^4\,5snp$; $3s^2\,3p^4\,4dnp$

Assignments to these higher series are possible for a few otherwise unknown resonances; however, no fully developed Rydberg series result. Obviously these assignments are questionable; however, their effective quantum numbers, as seen in Table IV(c), are reasonable.

4) $3s^2\,3p^4\,4pns$

Series of this type are apparently weaker – at least we are unable to pick out resonances which form good series in such configurations. Of course the first member $(4p\,4s)$ of such series have to be common with the first members of the $4snp$ series discussed in Sec. IV. B. (2) above. Hence it is necessary to look for members with $n\geq 5$ to establish the existence of resonances due to these configurations. Table IV(d) lists those resonances that are likely candidates for higher members of $4pns$ series. In only one case, $(^3P)4p(^2D_{3/2})ns$, have resonances been assigned to n values greater than 5. Note, however, that an alternative assignment is available for this Rydberg series as is discussed in the following paragraph.

5) $3s^2\,3p^4\,4pnd$

While the presence of series of this configuration seems reasonable, we can offer neither con-

firming assignments nor an explanation of their absence. Of course, the first members $4p\,3d$ exist since they are also first members of the $3dnp$ series listed in Table IV(a). However, we have been unable to establish higher Rydberg-series members converging to the required limits. A possible exception is the series formed by resonances (62), (64), and (66), which have been listed as the $n = 9-11$ members of the $(^3P)4p(^2D_{3/2})ns$ configuration in Table IV(d). However, it is not unreasonable, as an alternative, to assign these three resonances to the $n = 7-9$ members of a $(^3P)4p(^2D_{3/2})nd$ series to the same limit.

6) $3s^2\,3p^4\,4fns$; $3s^2\,3p^4\,4fnd$

The existence of such series has not been established and perhaps should not be expected, since two electrons are required to change angular momentum to form these configurations from the ground state.

C. Other Two-electron Excitation States

Transitions of the type $3p^6 \rightarrow 3p^4 nl\,n'l'$ cannot result in discrete resonances in the wavelength region below 285 Å since the energy involved would be sufficient to remove two of the outer p electrons. Hence the broad, low-contrast resonances seen in Fig. 2 must be due to higher-energy configurations. There are no one-electron excitation states available to explain these resonances (as mentioned earlier, the excitation of a $2p$ electron requires ~250 eV). It follows then, that the observed resonances are most likely due to two-electron excitation transitions of the type $3s^2 3p^6 \rightarrow 3s\,3p^5 nl\,n'l'$.

The grandparents of this two-electron excitation configuration are $3s\,3p^5(^{1,3}P)$. The most reasonable configurations of odd parity would be $3dns$, $4sns$, $4snd$, and $4pnp$, which require only one electron to change angular momentum and which can form $^1P_1$ final terms when L-S coupled to the grandparents. Thus we might expect to observe Rydberg series, converging onto excited states of Ar II, involving the configurations $3s\,3p^5 3d$, $3s\,3p^5 4s$, and $3s\,3p^5 4p$.

Note, however, that these configurations of Ar II are themselves auto-ionizing. They have not as yet been directly observed, and no calculations of their term energies exist. Further the excited states of Ar I involved here have, in general, *four incomplete subshells*, and thus their expected energies are difficult to estimate. We are not able to give a detailed interpretation of the spectra of Fig. 2 and have merely listed (Table V) the wavelength and wavenumber of the resonances which have been observed in the energy region appropriate to these configurations. Note that no Rydberg series develop. These resonances appear as weak absorption lines superimposed on the continuum, and their positions have been determined at the maximum absorption points.

TABLE V. Wavelength λ and wave number ν of all observed resonances which are due to two-electron transitions of the type $3s^2\,3p^6 \rightarrow 3s\,3p^5\,nl\,n'l'$. The error quoted represents the estimated probable error.

λ (Å)	ν (cm^{-1})
276.9 ± 0.2	361 100
271.1 ± 0.2	368 900
268.9 ± 0.2	371 900
258.6 ± 0.2	386 700
255.9 ± 0.2	390 800
254.4 ± 0.2	393 100
253.1 ± 0.2	395 100
252.3 ± 0.2	396 400
250.7 ± 0.2	398 900
247.5 ± 0.2	404 000
246.2 ± 0.2	406 200
244.4 ± 0.2	409 200
236.8 ± 0.2	422 300
220.0 ± 0.5	454 500
217.7 ± 0.5	459 300
216.2 ± 0.5	462 500
214.8 ± 0.5	465 500
213.4 ± 0.5	468 600

V. CROSS-SECTION DETERMINATIONS

A. Methods of Analysis

The spectra shown above were obtained utilizing a 3-m grazing-incidence spectrograph. All of the cross-section measurements, however, were obtained utilizing a 3-m grazing-incidence scanning monochromator[26] (Sec. II). Two methods were used to evaluate the argon photo-ionization cross-section data taken with this instrument. In regions where no resonances were present or if the resonances were broad compared to the optical slit width, the cross section was evaluated point-by-point from the transmission as a function of pressure. Where the effect of the slit was not negligible, a computerized method of data reduction was used that corrected for the smearing effect of the slit.

1) *Resonances Broad Compared to the Optical Slit Width*

The profiles of the $3s\,3p^6\,4p\ ^1P_1^\circ$ resonance and the two-electron resonance $(^3P)4s(^2P_{1/2})4p$ were quite broad and were determined by computing the cross section point-by-point through the resonance. Fifteen to 30 values of the transmission $T(\lambda, p)$ at a particular wavelength λ and pressure p were determined both from wavelength scans at a fixed pressure and from pressure scans at a fixed wavelength. Some background radiation, chiefly second order, was present. The cross section at wavelength λ and the fraction of background radiation could be determined (providing the magnitude of the cross section for the background radiation was known) by an iterative procedure.[28] In this method, the background and the cross section were adjusted until a plot of $\log[T_{\text{corrected}}(\lambda, p)]$ versus p was

a straight line through the origin, whose slope was proportional to the cross section at wavelength λ. The fraction of background radiation determined from this procedure decreased monotonically from 4.5 ±0.5% at 400 Å to 1.8 ±0.5% at 500 Å.

The magnitude of the cross section was determined with a probable error of ±5% from the data taken at each wavelength. The cross section was interpolated between wavelengths where it was evaluated, since the wavelength scans of the transmission used in the evaluation of the cross section were continuous.

All the resonances studied were fitted by Fano's[11, 21] parameterization of the cross section, which has the form

$$\sigma(E) = \sigma_a(q+\epsilon)^2/(1+\epsilon^2) + \sigma_b \qquad (1)$$

with $\epsilon = (E - E_\gamma)/\frac{1}{2}\Gamma$, where the quantities E and E_γ are the photon energy and the resonance energy ($\epsilon = 0$), respectively. The parameter q is the profile index[21] and is defined in terms of transition matrix elements between the ground state, the modified discrete state, and the continuum states. The half-width of the resonance is given by Γ, and the quantity σ_a is the cross section associated with the fraction of the available continua with which the discrete state interacts, while σ_b is the cross section associated with the fraction of continua which does not enter into the interaction. Equation (1) may also be written in terms of the total cross section $\sigma_T = \sigma_a + \sigma_b$ and the ratio $\rho^2 = \sigma_a/\sigma_T$, where ρ is the correlation index.[21] It should be mentioned that the magnitude of σ_T depends in detail on how the interaction redistributes the oscillator-strength density in the region of a resonance. For this reason, σ_T is not necessarily the cross section that would be measured in the absence of an interaction with the discrete state.

The parameters q, Γ, ρ^2, and σ_T were adjusted until a best fit was obtained by inspection. The errors in the parameters describing these resonances are, therefore, estimated errors. The quality of the fit of the data to the model cross section is an assurance that the theoretical model chosen is realistic.

2) *Resonances Not Broad Compared to the Optical Slit Width*

The optical slit width was an appreciable fraction of the resonance width for the second and third members of the $3s\,3p^6np\ {}^1P_1{}^\circ$ series and the $({}^3P)3d({}^2P_{3/2})4p$ two-electron excitation resonance, consequently the cross section in the region of these resonances is not necessarily proportional to the slope of the best straight line representing $\log[T(\lambda, p)]$ versus p.[5, 28] A computer program was devised to analyze the data, accounting for the smearing effect of the slit on the transmission. The spectrometer optical band pass function was taken to be a Gaussian of 0.065 Å full width at half maximum (f.w.h.m.). This form has been shown[35] to be a good approximation when the slit width and the diffraction width are the same (as is true for our monochromator). The computer program convolves the optical band pass function with the model transmission function computed from Eq. (1). The observed transmission is then compared with the computer predicted transmission. A nonlinear, least-squares, parameter-fitting routine[36] was used to fit the model transmission to the observed transmission. Each scan of the resonance at a fixed pressure was treated independently and values of q, ρ^2, Γ, and σ_T were determined from the set of parameters which minimized the sum of the square of the residuals. The computer routine also included a confidence limit calculation and estimated the standard deviation of each parameter. From this information the weighted average of the parameters was evaluated for each resonance and their standard deviation was computed.

An illustration of the method outlined above is shown in Fig. 5, where transmission measurements taken in the region of the $3s\,3p^6\,5p\ {}^1P_1{}^\circ$ resonance are compared with the predicted transmission. The plotting symbols O and ● were used on the computer "print out" to denote the observed and predicted transmission, respectively. If the observed and predicted values were coincident a ● is plotted. Figure 5 is a typical example of how well the model resonance profile fits the experimental data.

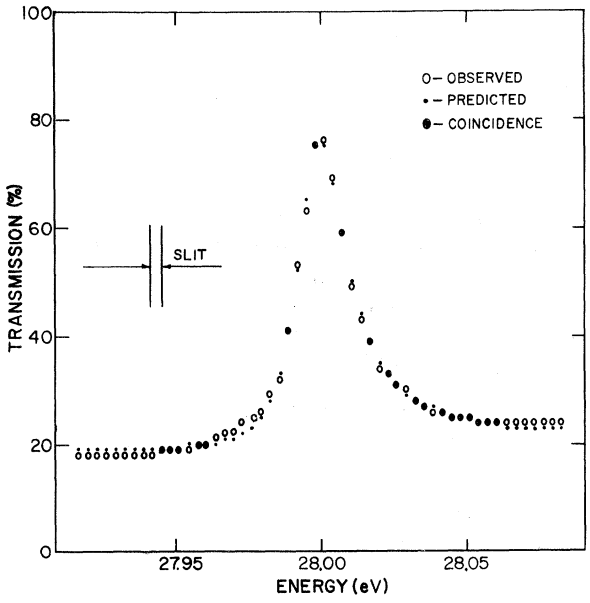

FIG. 5. An example of an experimental transmission profile of the $3s\,3p^6\,5p\ {}^1P_1{}^\circ$ resonance (denoted by the plotting symbol O) compared with the best model profile (denoted by the symbol ●) determined by the least-squares fitting routine. The plotting symbol ● is used to denote coincidence between the observations and the predicted transmission. The optical slit width is indicated on the figure and corresponds to the full width at half maximum of the Gaussian slit function used in the fitting routine. The average profile parameters, determined from a number of such transmission scans, are given in Table VI.

B. Resonance Profiles

1) *One-Electron Excitation Resonances, the* $3s\,3p^6np\ {}^1P_1{}^\circ$ *series*

Three members of this series were studied using the methods outlined above. In the case of the $3s\,3p^6\,5p\ {}^1P_1{}^\circ$ and $3s\,3p^6\,6p\ {}^1P_1{}^\circ$ resonances, 12 and 11 scans, respectively, were used with the parameter fitting routine to determine the values of q, ρ^2, Γ, and σ_T. For these resonances the value of the parameters and their standard deviation are tabulated in Table VI.

It should be mentioned that these resonances were analyzed in the framework of *noninteracting resonances*, i.e., each resonance was considered independent. Every member of this Rydberg series is expected to interact with the same continuum;[21] therefore the single noninteracting resonance cross section is an approximation. A representation in which the members of the series are allowed to interact with each other through the same continuum has been suggested by Fano[11] and used by Comes and Sälzer.[37] The cross section was calculated according to this form using the values of the experimentally determined parameters. Comparing the result with Eq. (1) revealed that the other resonances in the series contributed a negligible amount to the cross section in the vicinity of any given resonance. Thus the one resonance approximation is adequate for this analysis.

From Table VI it is clear that the quantity ρ^2 and the product $n^{*3}\Gamma$ are constant for these three series members within experimental error, and that the form of Γ is not $\Gamma = C\,n^*/(n^{*2}-1)^2$ as was suggested[38] in Ref. 21. The parameter q for this series is negative (as it was for the equivalent excitations in neon),[10] and its magnitude, while showing a tendency to decrease for higher-series members, is a constant within the limits of experimental error. The slight effect a 20% change in q has on the shape of the resonance profile can be seen in Fig. 6, where the profiles of the $3s\,3p^6\,4p\ {}^1P_1{}^\circ$ resonance ($q=-0.21$) and the $3s\,3p^6\,6p\ {}^1P_1{}^\circ$ resonance ($q=-0.17$) have been plotted. In each case, the cross section has been normalized to the background value σ_T, and the reduced energy $\epsilon = (E-E_r)/\frac{1}{2}\Gamma$ has been used as the abscissa scale.

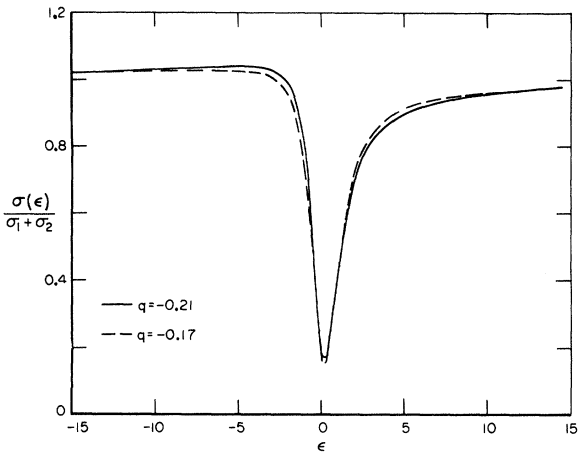

FIG. 6. Theoretical resonance profiles which best fit the $n=5$ and $n=6$ members of the $3s\,3p^6\,np\ {}^1P_1{}^\circ$ series. The figures show how the profile is affected as q changes from -0.21 (the $n=5$ series member) to -0.17 (the $n=6$ series member). The ordinate is the cross section normalized to the value of the cross section in the wings of the resonance, and the abscissa is the reduced energy $\epsilon = (E-E_0)\frac{1}{2}\Gamma$.

The classical spectroscopist is led naturally to ask what oscillator strength should be associated with these discrete resonant features. Since this is not, in general, a clear concept let us state our own view of the problem. In the case where the discrete level in question interacts with a vanishingly small portion of the underlying continua,[39] the area under the absorption maximum can be associated with the oscillator strength of the discrete state in the usual manner. However, when the discrete state in question interacts with a large fraction of the available continua, the integral of the excess absorption coefficient over the resonance no longer has the same meaning. In this case, the redistribution of the oscillator strength of the continua, due to interference effects, may make the resonant feature visible,

TABLE VI. Profile parameters experimentally determined for the first three members of the $3s\,3p^6\,np$ series and the two most prominent two-electron excitation resonances.

	$3s\,3p^6(^2S_{1/2})np\ {}^1P_1{}^\circ$			$3s^2\,3p^4(^3P)nl\,n'l'$	
	$(^2S_{1/2})4p\ {}^1P_1{}^\circ$	$(^2S_{1/2})5p\ {}^1P_1{}^\circ$	$(^2S_{1/2})6p\ {}^1P_1{}^\circ$	$(^3P)4s(^2P_{1/2})4p$	$(^3P)3d(^2P_{3/2})4p$
E (eV)	26.614	27.996	28.509	29.224	30.847
q	-0.22 ± 0.05[a]	-0.21 ± 0.02[b]	-0.17 ± 0.03[b]	-0.2 ± 0.1[a]	-1.9 ± 0.7[b]
Γ (eV)	0.080 ± 0.005	0.0282 ± 0.0013	0.0126 ± 0.0012	0.02 ± 0.01	0.006 ± 0.002
ρ^2	0.86 ± 0.04	0.83 ± 0.02	0.85 ± 0.03	0.10 ± 0.02	0.20 ± 0.03
σ_T (cm^{-1})[c]	940 ± 50	840 ± 40	800 ± 40	745 ± 40	600 ± 30
n^*	2.277	3.310	4.318		
$n^{*3}\Gamma$ (eV)	0.94 ± 0.05	1.02 ± 0.05	1.01 ± 0.10		

[a] The quoted errors for the parameters of this resonance are estimated probable errors.
[b] The quoted errors for the parameters of this resonance correspond to the standard deviation.
[c] σ_T is the background cross section extrapolated to the center of the resonance.

even prominent, far out of proportion to the inherent oscillator strength to be associated with the discrete transition in absence of its interaction with the continua. Further complications arise when more than one discrete state exists, and interactions between the discrete states can occur, either directly or through the continua with which they mutually interact. In essence, the oscillator strength is a poorly defined quantity of a resonance *whenever* the resonance interacts strongly with other configurations. Further insight into the complexities of this concept can be obtained by consulting the paper by Fano and Cooper[40] and Mies.[41]

2) *Two-Electron Excitation Resonances*

Profiles have been studied of two resonances which result from the simultaneous excitation of two $3p$ electrons. The Beutler-Fano profile parameters that have been determined for these resonances are tabulated in Table VI. Let us first consider the $(^3P)4s(^2P_{1/2})4p$ resonance that overlaps higher members of the $3s\,3p^6np\ ^1P_1^\circ$ series. This resonance is labeled (2) in Fig. 3 and appears as a weak and rather broad feature just below the $3s\,3p^6\,^2S_{1/2}$ limit. At this point in the one-electron excitation series ($n = 31$ at the peak transmission), the resonances are still separated by more than their Doppler widths and hence should still be a discrete series. We do not observe these as separate resonances,[42] since their separation is narrow in comparison with the optical slit width (0.06 Å). Thus we are unable to properly interpret the absorption in the region of resonance (2). Because of its small ρ^2, resonance (2) may have the shape which appears in Fig. 3 and be simply superimposed on the one-electron excitation series with little or no interaction; or, it might be that the $(^3P)4s(^2P_{1/2})4p$ level is in evidence only through its perturbing effect on the one-electron excitation series; or, some combination of these two extremes may prevail. In the case of the latter extreme, higher resolution would be expected to reveal no superposition of resonances but rather an intensity modulation of the high members of the $3s\,3p^6np\ ^1P_1^\circ$ series. For further discussion of this type of interaction consult Mies.[41]

The profile of the two-electron excitation resonance classified as $(^3P)3d(^2P_{3/2})4p$ has also been determined. Because this resonance was sharp compared to the optical slit width, the computerized data-fitting routine [Sec. V.A.(2)] was used to analyze the six transmission scans obtained for this resonance. The values of the parameters determined are listed in Table VI. This resonance has a relatively large negative q and a small ρ^2; hence it does not appear as prominent as the $3s\,3p^6np\ ^1P_1^\circ$ series. In Fig. 7, the profiles of these two resonances can be compared. Each resonance has been normalized to the background cross section σ_T, and the abscissa scale is in units of the reduced energy ϵ. The two-electron resonance with large negative q and small ρ^2 is denoted by B while the one-electron resonance with small negative q and large ρ^2 is denoted by A. Curve A is also appropriate for the other members of the $3s\,3p^6np\ ^1P_1^\circ$ series. From the densitometer traces in Figs. 3 and 4, it can be seen that a small value of ρ^2 and a negative q of order 2 characterize many of the two-electron excitation resonances.

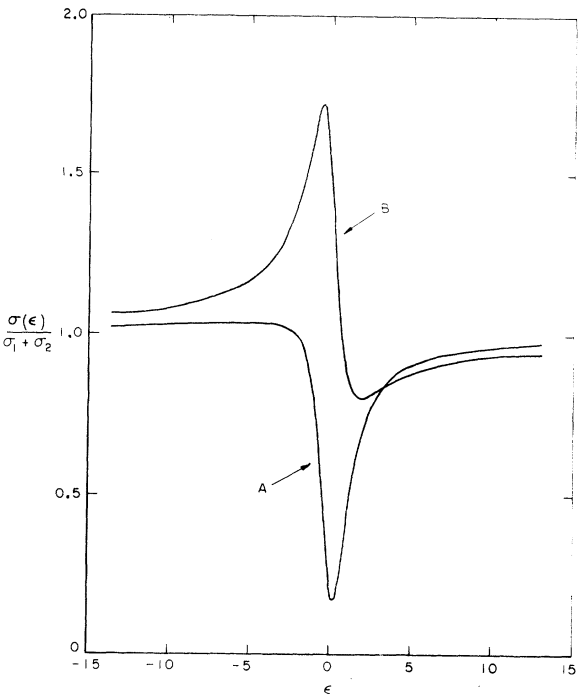

FIG. 7. Theoretical resonance profiles which best fit the experimentally observed shapes: (A) the single-electron excitation $3s\,3p^6\,4p\ ^1P_1^\circ$ and (B) the two-electron excitation $(^3P)3d(^2P_{3/2})4p$. The Beutler-Fano profile parameters which describe curves (A) and (B) are, respectively, $q = -0.22$, $\rho^2 = 0.86$ and $q = -1.9$, $\rho^2 = 0.20$.

C. Continuum Cross Section

The continuum photo-ionization cross section for argon has been measured in several investigations beginning with the work of Lee and Weissler[2] and Wainfan *et al.*[12] The region from the vicinity of the $3p^5\,^2P_{1/2,\,3/2}$ ionization limits to photon energies of 20 eV has been studied recently using the Hopfield continuum lamp.[3,4] Although the measurements of different laboratories were in agreement at threshold, at photon energies near 20 eV the results differ by 15 – 20%. Using spark sources the continuum cross-section has been studied from threshold to about 50 eV by Rustgi[18] and also Samson.[19] Above 50 eV, the cross section has been measured[15,43] at several laboratories.

If a line source is used for the determination of absorption cross sections in the presence of resonance structure, the structure may influence the observed magnitude of the background cross section in a way determined by the portion of the

resonance probed by the line radiation.

We have determined the average continuum cross section between about 22 and 35 eV using the synchrotron source. Most of the strong two-electron excitation resonances lie in the region of 28 to 38 eV and their effect on the photo-ionization cross section could be determined from monochromator wavelength scans in this energy region. Our measurements of the continuum cross section are shown in Fig. 8, while Fig. 9 is an expansion of the curve in the region of the $3s\,3p^6np\ ^1P_1^\circ$ series. Our measurements are indicated by the solid line. Where the cross section was evaluated point-by-point, the values of the cross section are plotted at the energy of measurement with the vertical bar indicating the magnitude of one standard deviation. In the region below 26 eV, where there is no structure (determined by examining spectrographic plates), the value of the cross section between the measured points can be represented by a smooth curve. Between 29 and 38 eV, we present the average background cross section without including the resonance structure.

In both Figs. 8 and 9, the resonance profiles of the first three members of the $3s\,3p^6np\ ^1P_1^\circ$ series and the $(^3P)4s(^2P_{1/2})4p$ two-electron resonance were calculated from Eq. (1) using the best experimentally determined values of the parameters q, ρ^2, Γ, and σ_T. The fit of the calculated curve to the cross section determined point-by-point through the $3s\,3p^6\,4p\ ^1P_1^\circ$ resonance can be seen in Fig. 9. In the region

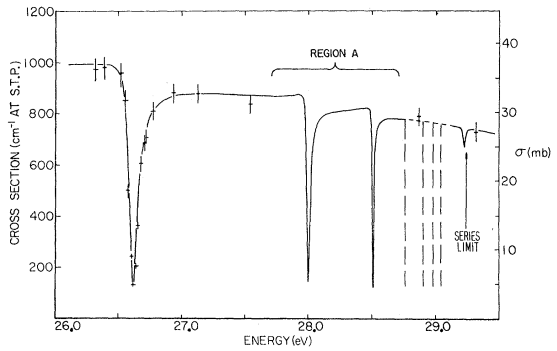

FIG. 9. An expanded view of the absorption cross section of argon in the region of the $3s\,3p^6\,np\ ^1P_1^\circ$ series. The cross section was evaluated point-by-point in the resonance profile of the $n=4$ member of the series. The error bars have a magnitude of one standard deviation. The solid line is the best fit of a Beutler-Fano profile to the data points. In region A the experimental data is described by the Beutler-Fano profile whose parameters were determined by the computerized parameter fitting technique. The vertical dashed lines indicate the position of the next-few-series members above $n=6$. The low contrast $(^3P)4s(^2P_{1/2})4p$ resonance just before the $3s\,3p^6\,np\ ^1P_1^\circ$ series limit is shown superimposed on the unresolved higher members of the series.

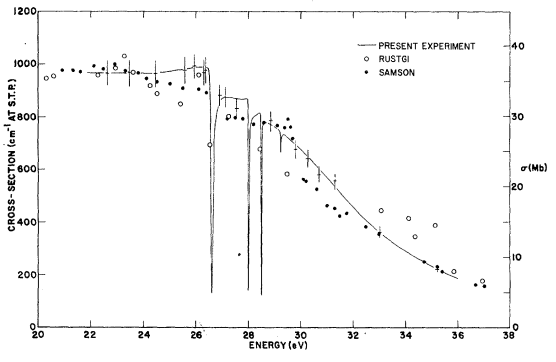

FIG. 8. The photo-ionization cross section of argon between 20 and 38 eV comparing the present measurements with the data of Rustgi (o) and Samson (•). In the present measurements the cross section was evaluated at discrete intervals in the continuous wavelength scans. The error bars on the data points have a magnitude of one standard deviation. The first three members of the $3s\,3p^6\,np\ ^1P_1^\circ$ series are shown, along with the second-lowest two-electron excitation, classified as $(^3P)4s(^2P_{1/2})4p$. The parameters which have been determined for these Beutler-Fano profiles are given in Table VI. At energies greater than 29 eV, there are many two-electron excitation resonances which are not shown here.

denoted as A in Fig. 9 only the computer method [Sec. V. A. (2)] was used to obtain the resonance profile from the experimental transmission. In Fig. 8, between the $n=7$ member of the $3s\,3p^6np\ ^1P_1^\circ$ series and the $(^3P)4s(^2P_{1/2})4p$ resonance, the cross section is shown dashed, since detailed cross-section measurements have not been made in this region.

The results of Rustgi[18] and Samson[19] are shown in Fig. 8 as open circles and dots, respectively. The background cross section is approximately constant with a value of 36.3 ±1.8 Mb (975 cm^{-1} at STP) between 18.5 eV and the $3s\,3p^6\,4p\ ^1P_1^\circ$ resonance, where it then begins to decrease approximately linearly with a slope of 2.8 Mb/eV throughout the $3s\,3p^6np\ ^1P_1^\circ$ series. In this region, the present value of the cross section is somewhat higher than any of the earlier work. Just beyond the $3s\,3p^6\ ^2S_{1/2}$ limit at a photon energy of 29.6 eV the continuum cross section determined by Samson decreases suddenly by 22%. We observe no such sudden decrease in the cross section, but find the cross section decreasing smoothly.

The continuum photo-ionization cross section for argon has been calculated by Cooper[44] and more recently by Conneely *et al.*[45] The calculation of Cooper used, basically, a one-electron Hartree-Fock potential to compute the wave function for the initial and final states, neglecting configuration interaction. Conneely *et al.* calculated the final-state wave function using the close-

coupling method.[46] Cooper's calculation predicts a cross section at threshold which is 2.5 times as large as that observed experimentally. According to Cooper, the cross section should decrease monotonically to a minimum at 43 eV (such a minimum is in fact observed[15, 43] at 48 eV) and a broad secondary maximum at higher photon energies. The dipole-length calculation of Conneely *et al.* qualitatively agrees with the experimental observations indicating a cross section that increases slightly with photon energy above threshold to a broad maximum and then decreases monotonically. However, the calculated maximum occurs about 8 eV above the observed maximum. Their dipole velocity calculation, on the other hand, gives values $\frac{1}{2}$ to $\frac{2}{3}$ that of experiment. Thus while some features of the continuum cross section have been accounted for theoretically, calculations of greater sophistication will apparently be required to bring the theoretical results into more quantitative agreement with the experimental data.

VI. CONCLUDING REMARKS

The classical scheme for the classification of spectra, which has been used here, cannot be expected to fully and properly account for the resonant features seen in the region above the ionization limit. Rather it is an approximation which is helpful in obtaining a starting analysis. Multiconfiguration interaction effects can mix the identity of observed resonance features and also distort resonance profiles. We hope this experimental work will be a useful testing ground for further theoretical advances, both in calculating the energies of two-electron excitation states from first principles, and in understanding the behavior of interacting resonances. We will attempt to provide photographs of the spectra to those who wish to extend this analysis.

---

*Contribution of the National Bureau of Standards not subject to copyright.

†Present address: The University of Reading, Reading, Berkshire, England.

[1]H. Beutler, Z. Physik 93, 177 (1935).

[2]P. Lee and G. L. Weissler, Phys. Rev. 99, 540 (1955).

[3]R. E. Huffman, Y. Tanaka, and J. C. Larrabee, J. Chem. Phys. 39, 902 (1963).

[4]P. H. Metzger and G. R. Cook, J. Opt. Soc. Am. 55, 516 (1965).

[5]R. D. Hudson and V. L. Carter, J. Opt. Soc. Am. 58, 227 (1968).

[6]W. A. Chupka and M. E. Russell, J. Chem. Phys. (to be published).

[7]R. P. Madden and K. Codling, Phys. Rev. Letters 10, 516 (1963).

[8]R. P. Madden and K. Codling, Autoionization: Astrophysical, Theoretical, and Laboratory Experimental Aspects, edited by Aaron Temkin (Mono Book Co., Baltimore, Md., 1966) p. 129.

[9]R. P. Madden and K. Codling, Astrophys. J. 141, 364 (1965).

[10]K. Codling, R. P. Madden, and D. L. Ederer, Phys. Rev. 155, 26 (1967).

[11]U. Fano, Phys. Rev. 124, 1866 (1961).

[12]N. Wainfan, W. C. Walker, and G. L. Weissler, Phys. Rev. 99, 542 (1955).

[13]G. L. Weissler, J. A. R. Samson, M. Ogawa, and G. R. Cook, J. Opt. Soc. Am. 49, 338 (1959).

[14]F. J. Comes and A. Elzer, Z. Naturforsch. 19a, 721 (1964).

[15]A. P. Lukirskii and T. M. Zimkina, Izv. Akad. Nauk. SSSR Ser. Fiz. 27, 817 (1963) [English transl.: Bull. Acad. Sci. USSR, Phys. Ser. 27, 808 (1963).]

[16]H. E. Blackwell, G. S. Bajwa, G. S. Shipp, and G. L. Weissler, J. Quant. Spectry. Radiative Transfer 4, 249 (1964).

[17]J. E. G. Wheaton, Appl. Opt. 3, 1247 (1964).

[18]O. P. Rustgi, J. Opt. Soc. Am. 54, 464 (1964).

[19]J. A. R. Samson, J. Opt. Soc. Am. 54, 420 (1964).

[20]J. A. R. Samson, Phys. Rev. 132, 2122 (1963).

[21]U. Fano and J. W. Cooper, Phys. Rev. 137, A1364 (1965).

[22]J. Arol Simpson, G. E. Chamberlain, and S. R. Mielczarek, Phys. Rev. 139, A1039 (1965).

[23]M. E. Rudd and D. V. Lang, Fourth International Conference on the Physics of Electronic and Atomic Collisions (Science Bookcrafters, Hastings-on-Hudson, New York, 1965), p. 153.

[24]K. Codling and R. P. Madden, J. Appl. Phys. 36, 380 (1965).

[25]A review of continuum light sources can be found in: G. V. Marr, Photoionization Processes in Gases (Academic Press, Inc., New York, 1967) pp. 62–64; see also P. Bogen, H. Conrads, G. Gatti, and W. Kohlhaas, J. Opt. Soc. Am. 58, 203 (1968), and references therein.

[26]R. P. Madden, D. L. Ederer, and K. Codling, Appl. Opt. 6, 31 (1967).

[27]L. Minnhagen, Arkiv Fysik 25, 203 (1963).

[28]D. L. Ederer, to be published.

[29]A. P. Lukirskii and T. M. Zimkina, Izv. Akad. Nauk. SSSR Ser. Fiz. 27, 324 (1963) [English transl.: Bull. Acad. Sci. USSR, Phys. Ser. 27, 333 (1963).]

[30]M. Nakamura, M. Sasanuma, S. Sato, M. Watanabe, H. Yamashita, Y. Iguchi, A. Ejiri, S. Nakai, S. Yamaguchi, T. Sagawa, Y. Nakai, and T. Oshio, Phys. Rev. Letters 21, 1303 (1968).

[31]A. Weiss, private communication.

[32]S. Goudsmit and L. Gropper, Phys. Rev. 38, 225 (1931).

[33]W. R. S. Garton in Autoionization: Astrophysical, Theoretical, and Laboratory Experimental Aspects, edited by Aaron Temkin (Mono Book Co., Baltimore, Md. 1966) p. 111.

[34]This resonance (13) has, in fact, a reasonable enough effective quantum number to be a second $5p$ member of the series $(^3P)4s(^2P_{3/2})np$, which is assigned in Table IV (b) to resonance (12). If we were to make this change,

however, no assignment seems to be available for resonance (12).

[35]P. C. von Planta, J. Opt. Soc. Am. 47, 629 (1957).

[36]This program is available in the Share Distribution Library (Share Distribution No. 1428.)
For an outline of the method see also D. W. Marquardt, J. Soc. Ind. Appl. Math. 11, 431 (1963).

[37]F. J. Comes and H. G. Sälzer, Phys. Rev. 152, 29 (1966).

[38]The authors of Ref. 21 have since withdrawn this suggested form of the dependence of Γ on n^*. Their discussion of this matter is contained in Ref. 40.

[39]The fraction of the underlying continua with which the discrete level can interact while still preserving the oscillator strength concept depends on the q of the resonance. The higher the q, the larger the fraction of the continua with which interaction can be tolerated.

[40]U. Fano and J. W. Cooper, Rev. Mod. Phys. 40, 441 (1968).

[41]F. H. Mies, Phys. Rev. 175, 164 (1968).

[42]In Fig. 3, the $3s\,3p^6\,np\,{}^1P_1{}^\circ$ series merges because of the finite width of the slit at about the level $n=20$. Above this point the slit transmits the intensity averaged over several resonances. The change in transmission registered by the detector at this point is a good approximation to the change in transmission that is observed beyond the series limit. This is not true for a series of sharp (compared to the slit) absorption resonances, where the transmission averaged over several resonances is a gross underestimate of the continuum transmission.

[43]R. W. Alexander, D. L. Ederer, and D. H. Tomboulian, Bull. Am. Phys. Soc. 9, 626 (1964).

[44]J. W. Cooper, Phys. Rev. 128, 681 (1962).

[45]M. Conneely, L. Lipsky, and K. Smith in Fifth International Conference on the Physics of Electronic and Atomic Collisions edited by I. P. Flaks and E. S. Solovyov (Nauka, Leningrad, 1967), p. 619.

[46]P. G. Burke and K. Smith, Rev. Mod. Phys. 34, 458 (1962).

PHYSICAL REVIEW VOLUME 177, NUMBER 1 5 JANUARY 1969

Photo-Ionization of Krypton Between 300 and 1500 eV. Relative Subshell Cross Sections and Angular Distributions of Photoelectrons*

Manfred O. Krause
Oak Ridge National Laboratory, Oak Ridge, Tennessee 37830
(Received 18 July 1968)

Energy spectra of electrons ejected from M and N subshells of krypton by characteristic x rays of 300 to 1500 eV energy have been measured with an electrostatic analyzer. Krypton was irradiated in the gas phase and electrons were detected perpendicular to the x-ray beam. From these spectra, relative subshell contributions to the photo-ionization cross section were obtained for single-electron emission and for double-electron emission, the latter involving simultaneous transitions of M and N electrons. Angular distributions of photoelectrons from $3s$, $3p$ and $3d$ shells of krypton and $1s$ shell of neon also have been determined at excitation energies from about 200 to 1100 eV above the respective ionization thresholds. Data on relative cross sections for single photo-ionization corroborate a theoretical model which uses a Herman-Skillman central potential (Cooper and Manson in the following article). Angular distributions agree satisfactorily with calculations by the same model; this means theory makes dependable predictions regarding the asymmetry parameter and the effect of retardation. Data on double photo-ionization disagree with results of the electron shakeoff theory which accounts for only about half the observed intensities. This suggests that electron-electron correlation plays an important role.

I. INTRODUCTION

Since the conception of the hydrogenic model of photo-ionization it has been known that this model would become increasingly inadequate with decreasing photon energy and increasing quantum number of the electrons.[1] Recent experimental studies[2–5] of total photoabsorption cross sections of rare gas atoms have shown its complete failure in the soft x-ray region. On the theoretical side[6] great improvements were achieved by using a more realistic central field than given in the hydrogenic approximation. Aside from causing the familiar sharp absorption edges to disappear, the new treatment[7,8] of photo-ionization resulted in irregular patterns of the individual subshell cross sections, both in magnitude and energy dependence, in contrast to the predictions of the hydrogenic model.[9] It is this behavior that makes measurements of subshell cross sections desirable, even on a relative basis, thus providing a direct test of specific results of theory. In the present study this was done by measuring the energy spectra of photoelectrons escaping from M and N subshells of krypton. Observation of photoelectrons from free atoms excluded complications arising from solid state or chemical effects and singled out photo-ionization events proper from other proces-

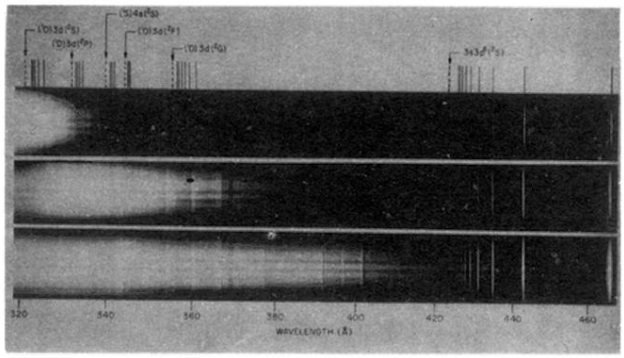

FIG. 1. Argon absorption spectrum between 320 and 470 Å taken at three different pressures to accentuate various regions of the spectrum (the background continuum cross section in this region varies by a factor of 5). This is a positive print so that black denotes absorption. The prominent series of window resonances on the right is due to the excitation of a subshell 3*s* electron to outer *p* orbitals. The other resonances are due to the simultaneous excitation of two 3*p* electrons. A few of the levels of Ar II to which Rydberg series of resonances have been seen are indicated on the figure at the upper left.

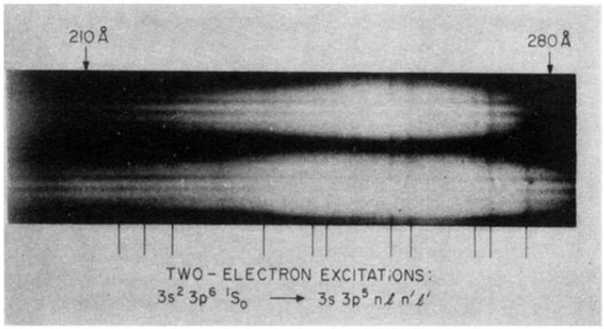

FIG. 2. Argon absorption spectrum between 200 and 280 Å showing two-electron excitations to states of the configurations $3s\ 3p^5\ nl\ n'l'$, which appear as weak absorption-type resonances. The vertical lines indicate the positions of some of the stronger features.